Ferromagnetic, *A*-Type, and Charge-Ordered CE-Type States in Doped Manganites Using Jahn-Teller Phonons

Seiji Yunoki, Takashi Hotta, and Elbio Dagotto

National High Magnetic Field Laboratory and Department of Physics, Florida State University, Tallahassee, Florida 32306

(Received 17 September 1999)

The two-orbital model for manganites with both noncooperative and cooperative Jahn-Teller phonons is studied at hole density $x = 0.5$ using Monte Carlo techniques. The phase diagram is obtained by varying the electron-phonon coupling and the t_{2g}-spins exchange. The insulating CE-type charge- and orbital-ordered state with the z-axis charge stacking observed in narrow-bandwidth manganites is stabilized in the simulations. Its charge gap $\Delta_{\rm CO}$ is much larger than the critical temperature $k_{\rm B}T_{\rm CO}$. Metalliclike *A*-type and ferromagnetic states are also obtained in the same framework, and the phase boundaries among them have first-order characteristics.

PACS numbers: 75.30.Kz, 71.10.–w, 75.10.–b

The complicated interplay between charge, spin, orbital, and lattice degrees of freedom is believed to induce the unexpected magnetic and transport phenomena observed in Mn oxides, such as the "colossal" magnetoresistance (MR) [1]. The subtle properties of manganites are especially complex at 50% hole density where experiments have established that an insulating charge-ordered (CO) state exists in $Nd_{0.5}Sr_{0.5}MnO_3$ [2], $Pr_{0.5}Ca_{0.5}MnO_3$ [3], $LaSr_2Mn_2O_7$ [4], and several others. The state has alternating $d_{3x^2-r^2}/d_{3y^2-r^2}$ orbital and CE-type antiferromagnetic (AF) order, and it corresponds to the complex charge, spin, and orbital arrangement [Fig. 1(d)] predicted in the 1950s by Goodenough [5]. Its melting by a magnetic field leads to a huge negative MR [6], probably induced by mixed-phase tendencies [7,8].

In spite of its importance, the origin of the $x = 0.5$ CO state is still unclear. The observation of charge populating only the even (or odd) Mn-ion sublattice in the xy plane naively suggests that the nearest-neighbor (NN) Coulomb repulsion $V_{\rm NN}$ is important for its stabilization. However, the z-axis stacking of charge [9] and existence of bistripes at $x > 0.5$ [10], both penalized by a strong NN repulsion, show that $V_{\rm NN}$ is smaller than expected and other ingredients are needed to understand the CO state [11]. In addition, at $x = 0.5$ experiments exhibited two other phases in competition: (i) A $d_{x^2-y^2}$ orbital-ordered (OO) but charge-disordered (CD) state with an *A*-type spin arrangement and two-dimensional (2D) metallicity (in, e.g., $Pr_{0.5}Sr_{0.5}MnO_3$ [2]). This *A*-type order has antiparallel spins along one direction and parallel in the other two. (ii) A metallic spin ferromagnetic (FM) CD and orbital-disordered (OD) state (in, e.g., $La_{0.5}Sr_{0.5}MnO_3$). For a dominant $V_{\rm NN}$, stable CD states at $x = 0.5$ are difficult to understand. It may occur that electrons coupled only through on-site Coulomb interactions produce this exotic behavior [12]. However, in this context unbiased many-body calculations are difficult. In addition, the colossal oxygen isotope shift of the CO transition in $Nd_{0.5}Sr_{0.5}MnO_3$ (NSMO) [13] cannot be explained using purely Coulombic approaches.

Searching for an alternative mechanism to stabilize the charge-stacked CO state of manganites, in this paper the first comprehensive computational analysis of the half-doped two-orbital model with both noncooperative and cooperative Jahn-Teller (JT) phonons in the large electron-phonon coupling (λ) regime is presented. Our main result is that a CE-type CO orbital-ordered ground state can be stabilized in this framework with charge properly stacked along the z axis.

The two-orbital Hamiltonian is given by

$$H = -\sum_{\mathbf{i}\mathbf{v}\sigma ab} t_{ab}^{\mathbf{v}} c_{\mathbf{i}a\sigma}^{\dagger} c_{\mathbf{i}+\mathbf{v}b\sigma} - J_{\rm H}\sum_{\mathbf{i}} \mathbf{S_i}\cdot\mathbf{s_i} + J_{\rm AF}\sum_{\langle\mathbf{ij}\rangle} \mathbf{S_i}\cdot\mathbf{S_j} + \lambda\sum_{\mathbf{i}ab\sigma} c_{\mathbf{i}a\sigma}^{\dagger}(Q_{2\mathbf{i}}\sigma_1 + Q_{3\mathbf{i}}\sigma_3)_{ab} c_{\mathbf{i}b\sigma} + \frac{1}{2}\sum_{\mathbf{i}}(Q_{2\mathbf{i}}^2 + Q_{3\mathbf{i}}^2), \quad (1)$$

where $c_{\mathbf{i}1\sigma}$ ($c_{\mathbf{i}2\sigma}$) is the destruction operator for an e_g electron with spin σ in the $d_{x^2-y^2}$ ($d_{3z^2-r^2}$) orbital at site $\mathbf{i}$, $\mathbf{v}$ is the vector connecting NN sites, and $t_{ab}^{\mathbf{v}}$ is given by $t_{11}^{\mathbf{x}} = -\sqrt{3}\,t_{12}^{\mathbf{x}} = -\sqrt{3}\,t_{21}^{\mathbf{x}} = 3t_{22}^{\mathbf{x}} = t$ (energy unit) for $\mathbf{v} = \mathbf{x}$, $t_{11}^{\mathbf{y}} = \sqrt{3}\,t_{12}^{\mathbf{y}} = \sqrt{3}\,t_{21}^{\mathbf{y}} = 3t_{22}^{\mathbf{y}} = t$ for $\mathbf{v} = \mathbf{y}$, and $t_{22}^{\mathbf{z}} = 4t/3$, $t_{11}^{\mathbf{z}} = t_{12}^{\mathbf{z}} = t_{21}^{\mathbf{z}} = 0$ for $\mathbf{v} = \mathbf{z}$. The Hund coupling $J_{\rm H}(>0)$ links the e_g-electron spin $\mathbf{s_i} = \sum_{a\alpha\beta} c_{\mathbf{i}a\alpha}^{\dagger}\boldsymbol{\sigma}_{\alpha\beta}c_{\mathbf{i}a\beta}$ and the localized t_{2g}-spin $\mathbf{S_i}$ assumed classical ($|\mathbf{S_i}| = 1$). The e_g-electron density $\langle n\rangle$ varies with a chemical potential μ (the hole density is $x = 1 - \langle n\rangle$). $J_{\rm AF}$ is the AF coupling between NN t_{2g}-spins. The fourth term couples e_g electrons to JT-mode distortions, $Q_{2\mathbf{i}}$ and $Q_{3\mathbf{i}}$, assumed classical [8,14]. σ_1 and σ_3 are Pauli matrices. When the $\{Q\}$ are independent, "noncooperative" phonons are used [8,14]. In real materials, however, adjacent MnO_6 octahedra share an oxygen. In this "cooperative" case, the proper variables

 0031-9007/00/84(16)/3714(4)$15.00

are the oxygen displacements $u_{\mathbf{i}}^{\mathbf{v}}$ from equilibrium along the Mn-Mn bond in the $\mathbf{v}$ direction, and extra terms are added to Eq. (1) for the breathing-mode phonon [15]. Standard Monte Carlo (MC) simulations for the classical spins and phonons are here used [8].

Figure 1(a) already illustrates one of the main results of the present study. Shown are the MC real-space charge correlations at $x = 0.5$ for representative couplings in 2D at low temperature (T). For intermediate J_{AF} ($0.1 \lesssim J_{\mathrm{AF}} \lesssim 0.2$), the charge correlations were found to be robust at all distances and they are positive (negative) on the even (odd) sites, compatible with the CO pattern observed in $x = 0.5$ experiments. Our results show that this behavior is essentially independent of λ for intermediate J_{AF}, although the CO pattern is more easily observed for large λ. For small J_{AF} ($\lesssim 0.1$), on the other hand, the CO state appears only for large λ. The observed CO state originates from the tendency of the JT-distorted Mn^{3+} ions to maximize their relative distances to exploit the kinetic energy of the mobile carriers. Figure 1(b) contains the Fourier transform of the t_{2g} spin correlations $S(\mathbf{q})$ in the CO regime. For intermediate J_{AF}, peaks at $\mathbf{q} = (\pi, 0)$ and $(\pi/2, \pi/2)$ are observed in excellent agreement with the result of a perfect CE-spin arrangement. Note that size effects appear small in these calculations, and throughout the paper. For small J_{AF}, only one peak is detected at $\mathbf{q} = (0, 0)$, indicating the FM phase. Under the CE-type spin environment, it can be shown that the CO state is stable even for small λ, since the system is effectively one-dimensional (1D) due to charge confinement along the zigzag FM chain [16]. In this sense, J_{AF} plays a role more important than λ for the CE-state stabilization. This is in contrast to the FM state

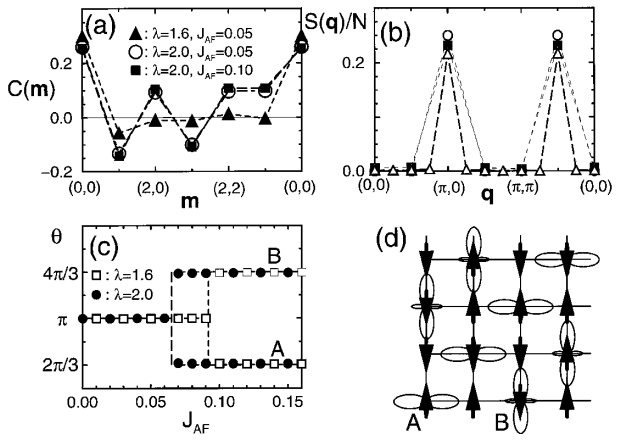

FIG. 1. (a) Charge correlation $C(\mathbf{m}) = \langle n_{\mathbf{i}} n_{\mathbf{i+m}} \rangle - \langle n \rangle^2$ with $n_{\mathbf{i}} = \sum_{a\sigma} c^{\dagger}_{\mathbf{i}a\sigma} c_{\mathbf{i}a\sigma}$ for $J_{\mathrm{H}} = \infty$, $T = 1/100$, and $x = 0.5$, using a 4×4 cluster with noncooperative phonons and periodic boundary conditions. The squares (circles) [triangles] were obtained at $J_{\mathrm{AF}} = 0.1$, $\lambda = 2.0$ (0.05, 2.0) [0.05, 1.6]. (b) Spin structure factor $S(\mathbf{q}) = \sum_{\mathbf{m}} e^{i\mathbf{q}\cdot\mathbf{m}} \langle \mathbf{S}_{\mathbf{i}} \cdot \mathbf{S}_{\mathbf{i+m}} \rangle$ for the t_{2g} spins at the same parameters of the squares in (a). The squares (circles) here denote the 4×4 MC (ideal CE-type state) results. Triangles are MC results on an 8×8 cluster. (c) $\theta_{\mathbf{A}}$ and $\theta_{\mathbf{B}}$ (see text) vs J_{AF} for $\lambda = 1.6$ and 2.0. (d) Charge, spin, and orbital arrangements are compatible with our MC results.

where a finite and large λ is needed to stabilize the CO state due to its higher dimensionality.

Regarding the orbital arrangement, let us consider sites with substantial charge [A and B in Fig. 1(d)]. The occupied orbital at each site is given by $|\tilde{2}\rangle_{\mathbf{i}} = -\sin(\theta_{\mathbf{i}}/2)|1\rangle + \cos(\theta_{\mathbf{i}}/2)|2\rangle$ with $\theta_{\mathbf{i}} = \tan^{-1}(\langle Q_{2\mathbf{i}} \rangle / \langle Q_{3\mathbf{i}} \rangle)$. In Fig. 1(c), θ_{A} and θ_{B} vs J_{AF} are plotted for $\lambda = 1.6$ and 2.0. For small J_{AF}, $\theta_{\mathrm{A}} = \theta_{\mathrm{B}} = \pi(d_{x^2-y^2})$, since the orbitals prefer to have large overlaps in both the x and the y directions. On the other hand, for intermediate J_{AF}, $\theta_{\mathrm{A}} = 2\pi/3(d_{3x^2-r^2})$ and $\theta_{\mathrm{B}} = 4\pi/3(d_{3y^2-r^2})$ since the orbitals are polarized along the hopping direction to improve the kinetic energy. Because of this effect, the zigzag hopping path in the CE-type CO state induces the alternating $d_{3x^2-r^2}/d_{3y^2-r^2}$ orbitals. The above results in charge, spin, and orbital correlations for intermediate J_{AF} are schematically shown in Fig. 1(d), which is the CE-type CO state observed in experiments. Note that the CE state found here is the *overall* ground state. For instance, 1D paths along straight lines have larger energy. The zigzag paths of the CE state are particularly stable due to their band-insulator character at $\lambda = 0$ [16].

Figure 2(a) shows a typical MC energy vs J_{AF} for $\lambda = 1.5$. At small J_{AF}, a FM state is stabilized since even at large λ the optimal background for electrons has all spins aligned. However, its energy is penalized by the AF exchange and at realistic values of J_{AF} an equal AF-FM mixture such as the CO CE state minimizes the energy. The discontinuity in $d(E/N)/dJ_{\mathrm{AF}}$ signals a *first-order* transition, as in experiments. With increasing J_{AF}, the CE state is destabilized by a novel state labeled "AF(2)" [17]. The metallic vs insulating character of the various phases can be analyzed with the Drude weight D_W [8]. Results at $\lambda = 1.2$ [Fig. 2(b)] show that the FM state is metallic ($D_W \neq 0$) and the CE state is insulating ($D_W = 0$). The jump in D_W again signals a first-order transition. Based on results similar to those in Figs. 2(a) and 2(b), the phase diagram in 2D and low-T was constructed [Fig. 2(c)]. It presents a rich structure including FM and CE phases. In particular, it contains a CD FM state with *uniform* orbital order, which after consideration of three-dimensional (3D) clusters will become a fully A-type state with charge and orbital characteristics as observed experimentally [2]. Then, all the currently known states at $x = 0.5$ exist in our phase diagram, and they are in close competition. It is conceivable that small temperature, doping, or lattice spacing changes may alter their balance, as found experimentally. It is also possible that the other novel phases in Fig. 2(c), especially the CO and OO FM state, may appear in future experiments.

Consider now cooperative effects. When the oxygen positions $\{u_{\mathbf{i}}^{v}\}$, not $\{Q\}$, are used as variables in the MC simulations, the charge, spin, and orbital correlations are found to be similar to the noncooperative results. In particular, a clear evidence of a CO CE-type state was observed in a wide range of the phase diagram, and to stabilize this state J_{AF} is crucial as in the noncooperative case. For $J_{\mathrm{AF}} = 0$, a CO state is still obtained at large λ, but it is spin FM.

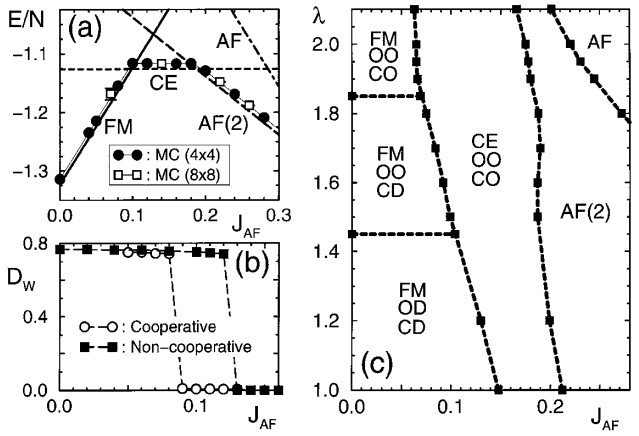

FIG. 2. (a) MC energy per site E/N vs J_{AF} at $x = 0.5$, $\lambda = 1.5$, $T = 1/100$, and $J_{\mathrm{H}} = \infty$ with noncooperative phonons. The FM state is charge disordered and orbital (uniform) ordered. "AF(2)" is explained in Ref. [17]. "AF" is AF in both directions. The straight lines correspond to the finite J_{AF} correction to $J_{\mathrm{AF}} = 0$ MC results, when a perfect spin configuration is assumed. (b) Drude weight D_W vs J_{AF} at $T = 1/100$, $x = 0.5$, using a 4×4 cluster. The results with cooperative (noncooperative) JT phonons were obtained at $\lambda = 1.5$ (1.2). (c) Phase diagram of the 2D two-orbital model with noncooperative phonons at low T. The phase boundaries were obtained as in (a) using 4×4 and 8×8 clusters. All transitions are of first order. In the FM phases, the OO state is $d_{x^2-y^2}$ uniform, while in the CE phase the pattern Fig. 1(d) was observed.

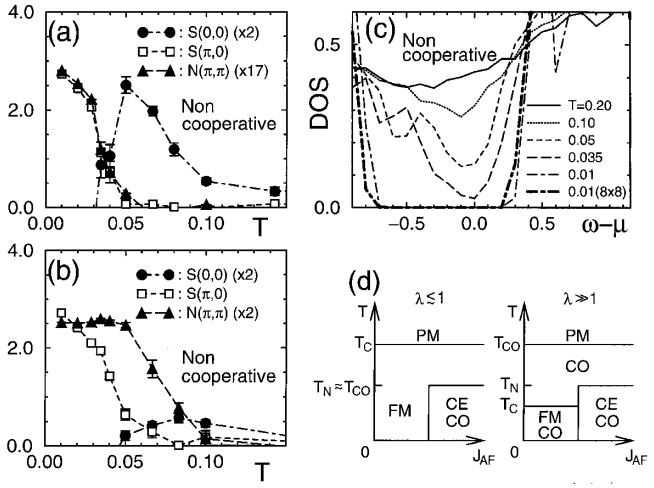

FIG. 3. (a) Spin structure factors $S(0,0)$ and $S(\pi,0)$ and charge structure factor $N(\pi,\pi)$ vs T for a 4×4 cluster with $\lambda = 1.2$ and $J_{\mathrm{AF}} = 0.15$. The high-T background, corresponding to on-site correlations only, is subtracted. (b) Same as (a) but at $\lambda = 1.9$ and $J_{\mathrm{AF}} = 0.10$. (c) DOS vs ω for 4×4 and 8×8 clusters for $J_{\mathrm{AF}} = 0.15$ and $\lambda = 1.2$. (d) Schematic phase diagram in the (J_{AF}, T) plane for the small λ (left) and large λ (right) regions. PM means paramagnetic phase.

In addition, note that the A-type phase of Fig. 2(c) has Q_3 modes with a *uniform* mean value at every site. This amounts to a static deformation of the oxygen octahedra [18]. If appropriate lattice constants are not used for cooperative phonons, the A-type phase may not be stabilized.

It is instructive to calculate the T dependence of the various order parameters to compare with experiments. In Fig. 3(a), $S(\mathbf{q})$ at $\mathbf{q} = (0,0)$ (FM) and $(\pi,0)$ (CE), and charge structure factor $N(\pi,\pi)$ vs T are shown for an intermediate λ. At $T \sim 0.1t$, $S(0,0)$ grows with reducing T as if FM were to become stable. However, at $T_{\mathrm{CO}} \sim T_{\mathrm{N}} \sim 0.05t$ a *sudden* transition to a CO CE state is found ($T_{\mathrm{CO}} \sim 250$ K for $t \sim 0.5$ eV). Note that the appearance of ferromagnetism in a temperature window above T_{CO} is in quantitative agreement with results observed in $La_{0.5}Ca_{0.5}MnO_3$ (LCMO) [19], and in $(La_{1-z}Nd_z)_{0.5}Sr_{0.5}MnO_3$ (LNSMO) for $z \geq 0.6$ [18]. The results at large λ are *qualitatively* different [Fig. 3(b)]. Here $T_{\mathrm{CO}} > T_N$, and only a weak FM signal is observed. These results are in good agreement with experiments for $La_{0.5}Sr_{1.5}MnO_4$ [20] and $Pr_{0.5}Ca_{0.5}MnO_3$ [3]. No metallic FM state exists in these compounds, and our analysis predicts that they will have a larger λ than LCMO and LNSMO [21]. The density of states (DOS) at several T's are in Fig. 3(c). A robust charge gap $\Delta_{\mathrm{CO}} \sim 0.9t$ at $T \sim 0.01t$ is clear, as well as a precursor pseudogap at higher T's. The ratio $\Delta_{\mathrm{CO}}/k_{\mathrm{B}}T_{\mathrm{CO}} \sim 18$ is remarkably close to the tunneling results ($\sim$19) for NSMO [22].

Let us understand intuitively the several transition temperatures. In the small λ region, the FM transition temperature T_{C} scales with t due to the double exchange mechanism, while T_{N} is determined by J_{AF} irrespective of λ. In the FM phase, a CO state never occurs in this region. However, if a sharp transition to the CE-type AF state occurs at $T = T_{\mathrm{N}}$, the CO state is also generated, since the CE-type state is a 1D band insulator [16], and it can be shown using a mean-field approximation that $k_{\mathrm{B}}T_{\mathrm{CO}} \approx \varepsilon_F e^{-1/\lambda}$, where ε_{F} is the Fermi energy much larger than J_{AF}. Thus, $T_{\mathrm{CO}} \sim T_{\mathrm{N}}$ holds for small λ. Note that $\Delta_{\mathrm{CO}}/k_{\mathrm{B}}T_{\mathrm{CO}}$ is large because $\Delta_{\mathrm{CO}} \sim t$ in the band-insulating region. When λ is increased, Δ_{CO} and T_{CO} smoothly increase, keeping $\Delta_{\mathrm{CO}} \gg k_{\mathrm{B}}T_{\mathrm{CO}}$. Eventually, at large λ, T_{CO} overcomes T_{N}. In this regime, T_{C} is determined by the superexchange mechanism as $T_{\mathrm{C}} \sim t/\lambda^2$. The above estimations are summarized in Fig. 3(d). In the small λ region, the metallicke FM phase appears irrespective of J_{AF} at high T, but at low T, the CE-type AF state occurs for intermediate J_{AF}'s and the CO state is concomitant only to the CE phase. In the large λ regime, the CO state occurs in the whole region for $T < T_{\mathrm{CO}}$, higher than T_{C} and T_{N}. At low T, the system becomes the FM insulator or CE-type insulator depending on J_{AF}. All these results are supported by the MC simulations. Note that previously it was widely believed that modifications in the tolerance factor t_{F} by chemical substitution lead to bandwidth changes sufficiently strong to drastically affect the properties of manganite compounds. However, our results established that the t_{F}-induced changes in J_{AF} are equally important, and they should be carefully considered when studying Mn oxides.

A difficult to understand feature of the manganite CO state is the z-axis charge stacking. To address the prediction of JT-phonon studies, in Fig. 4(a) the MC energy of a bilayer cluster vs J_{AF} with noncooperative

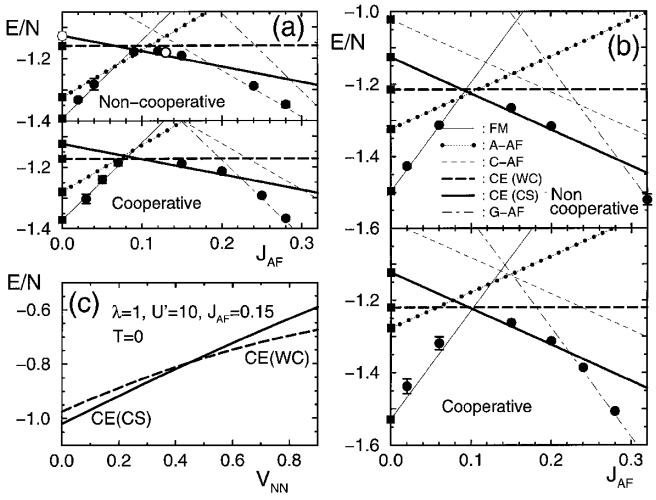

FIG. 4. (a) Energy per site vs $J_{\rm AF}$ at $\lambda = 1.5$, $J_{\rm H} = \infty$, and $T = 1/100$ with both cooperative and noncooperative phonons. Solid (open) circles are MC results using a $4 \times 4 \times 2$ ($8 \times 8 \times 2$) bilayer. Squares at $J_{\rm AF} = 0$ are the MC results on the $4 \times 4 \times 2$ cluster assuming the t_{2g}-spin background according to the convention in (b), in a standard notation. The straight lines were obtained as in Fig. 2(a). (b) Same as (a) but for a cube 4^3. Note that with noncooperative phonons the A-type phase is stable in bilayers and cubes in a narrow $J_{\rm AF}$ window. (c) Mean-field energy per site vs $V_{\rm NN}$ for a bilayer. Couplings are realistic (U' is the on-site interorbital repulsion). Since $J_{\rm H}$ is assumed infinite, the on-site intraorbital repulsion is irrelevant. Solid and dashed curves denote the CE-type CS and WC structures, respectively.

phonons is shown. At small $J_{\rm AF}$ the FM state dominates, as in 2D [Fig. 2(c)]. The CE state in its "Wigner crystal" (WC) and "charge stacked" (CS) versions [with a $N(\mathbf{q})$ peak at (π, π, π) and $(\pi, \pi, 0)$, respectively] appear as excited states at $J_{\rm AF} = 0$. WC has lower energy since the electronic kinetic energy improves when the Mn^{3+} ions spread apart. However, with increasing $J_{\rm AF}$ the situation rapidly changes since the CS charge arrangement (CE planes, one over the other, with opposite spins) has all z-axis bonds properly antiferromagnetically aligned. On the other hand, in the WC arrangement, with one plane shifted from the other by a lattice spacing along x or y, half the z-axis bonds are AF and the other half FM, making its energy $J_{\rm AF}$ independent. For this reason, at realistic $J_{\rm AF}$, the CS state dominates. Since similar results are obtained with cooperative phonons and cubic clusters [Fig. 4(b)], the effect appears robust and independent of fine details. The important interaction to stabilize the CS state is the z-axis $J_{\rm AF}$ exchange.

The $V_{\rm NN}$ repulsion will certainly penalize the CS structure, and the WC state will eventually become the ground state as this repulsion grows. However, the CS state has a better magnetic energy than the WC state. Comparing the energy per site gained ($-J_{\rm AF}$) and lost ($V_{\rm NN}/2$) in the 3D CS structure, a critical coupling $V_{\rm NN}^c = 2J_{\rm AF} \sim 0.15$ eV is estimated if $J_{\rm AF} \sim 0.15t$ and $t \sim 0.5$ eV. A more sophisticated mean-field approximation [23,24] at realistic manganite couplings provides $V_{\rm NN}^c \sim 0.22$ eV [Fig. 4(c)]. Although the $V_{\rm NN}$ bare value is $\sim$3.6 eV, it is reduced by the dielectric constant $\epsilon \approx 20$–45 [25], leading to $V_{\rm NN} \approx 0.08$–0.18 eV for manganites. Thus, it is concluded that the manganite NN repulsion is weak enough to allow for the CS state to be stable due to the effect of $J_{\rm AF}$ [26].

In summary, evidence was provided that the CE-type CO state with $\Delta_{\rm CO}/k_B T_{\rm CO} \gg 1$ and charge stacked along the z axis observed at $x = 0.5$ in several manganites can be stabilized using JT phonons. The competing FM and A-type states also appear in the simulations. Our results have established that purely Coulombic approaches are not the only procedure to stabilize CO states in manganites, but strongly coupled electron JT-phonon systems provide an alternative framework where controlled many-body calculations are possible. In addition, here it has also been established that the FM-CO/AF transitions are of first order, a key result upon which the addition of disorder leads to giant coexisting cluster formation and percolative behavior, as observed in experiments [27].

E. D. is supported by Grant No. NSF-DMR-9814350.

[1] S. Jin *et al.,* Science **264**, 413 (1994).
[2] H. Kawano *et al.,* Phys. Rev. Lett. **78**, 4253 (1997).
[3] Y. Tomioka *et al.,* Phys. Rev. B **53**, R1689 (1996).
[4] J. Q. Li *et al.,* Phys. Rev. B **57**, R3205 (1998).
[5] J. B. Goodenough, Phys. Rev. **100**, 564 (1955).
[6] Y. Tokura *et al.,* Phys. Rev. Lett. **76**, 3184 (1996).
[7] S. Yunoki *et al.,* Phys. Rev. Lett. **80**, 845 (1998); A. Moreo *et al.,* Science **283**, 2034 (1999).
[8] S. Yunoki *et al.,* Phys. Rev. Lett. **81**, 5612 (1998).
[9] E. Wollan and W. Koehler, Phys. Rev. **100**, 545 (1955).
[10] S. Mori *et al.,* Nature (London) **392**, 473 (1998).
[11] Y. Moritomo *et al.,* Phys. Rev. B **56**, 14 879 (1997).
[12] T. Mizokawa and A. Fujimori, Phys. Rev. B **56**, R493 (1997).
[13] G. Zhao *et al.,* J. Phys. Condens. Matter **10**, L737 (1998).
[14] A. J. Millis *et al.,* Phys. Rev. Lett. **74**, 5144 (1995).
[15] T. Hotta *et al.,* Phys. Rev. B **60**, R15 009 (1999).
[16] T. Hotta *et al.,* Int. J. Mod. Phys. B **12**, 3437 (1998); T. Hotta *et al.,* Phys. Rev. Lett. **84**, 2477 (2000).
[17] The AF(2) state has t_{2g} spins arranged as ↑↑↓↓ periodically along the x axis. Along the y axis the spins are AF.
[18] T. Akimoto *et al.,* Phys. Rev. B **57**, R5594 (1998).
[19] P. Schiffer *et al.,* Phys. Rev. Lett. **75**, 3336 (1995).
[20] B. J. Sternlieb *et al.,* Phys. Rev. Lett. **76**, 2169 (1996).
[21] In the $T \to 0$ CE-stable region, the FM signal weakens as $J_{\rm AF}$ increases at fixed λ.
[22] A. Biswas *et al.,* J. Phys. Condens. Matter **9**, L355 (1997).
[23] To be described elsewhere.
[24] The Coulomb interactions may play a role as important as the JT terms. However, mean-field-level approximations [15,16] support the view that pure-JT and pure-Coulombic calculations lead to qualitatively similar results [8].
[25] T. Arima and Y. Tokura, J. Phys. Soc. Jpn. **64**, 2488 (1995); J. H. Jung (private communication).
[26] Values of $J_{\rm AF}$ around $0.1t$, as found here to stabilize the CE phase, are realistic. For a discussion see Ref. [15].
[27] A. Moreo *et al.,* cond-mat/9911448.